

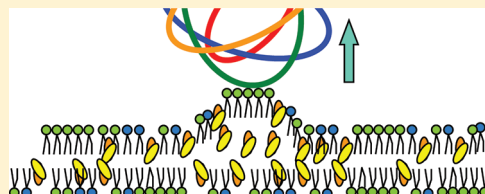
## Nanomechanical Recognition of Sphingomyelin-Rich Membrane Domains by Atomic Force Microscopy

Tong Wang,<sup>†,‡</sup> Hidehiko Shogomori,<sup>†,‡</sup> Masahiko Hara,<sup>†,‡</sup> Taro Yamada,<sup>\*,‡</sup> and Toshihide Kobayashi<sup>\*,†,‡,§</sup>

<sup>†</sup> RIKEN Frontier Research System and <sup>‡</sup> RIKEN, Advanced Science Institute, Saitama 351-0198, Japan

<sup>§</sup> INSERM U1060, INSA-Lyon, Villeurbanne, France

**ABSTRACT:** Sphingomyelin (SM) is a reservoir of signaling lipids and forms specific lipid domains in biomembranes together with cholesterol. In this study, atomic force microscopy (AFM) and force measurement were applied to investigate the interaction of SM-binding protein toxin, lysenin, with *N*-palmitoyl-*D-erythro*-sphingosylphosphorylcholine (palmitoyl sphingomyelin, PSM) bilayer spread over a mica substrate, in an aqueous buffer solution. Lysenin molecules were grafted on a silicon nitride tip for AFM by siloxane–thiol–amide coupling. The bilayers were prepared by the Langmuir–Blodgett (LB)/Langmuir–Schaefer (LS) method. By repeating cycles of tip approach/retraction motion, single-molecular adhesion motions were observed on the force curve, characterized as “fishing curves”. The addition of cholesterol and 1,2-dioleoyl-*sn*-glycero-3-phosphocholine (DOPC) did not alter the peak force but increased the peak extension. Mixtures of PSM/DOPC/cholesterol exhibited 2-dimensional two-phase domain separation. The characteristic fishing curves were observed exclusively in one of the phases, indicating the selective interaction of the lysenin tip to PSM-rich membrane domains. Our results indicate that the AFM tips conjugated with lysenin are useful to detect the surface distribution of SM-rich membrane domains as well as the nanomechanical properties of the domains.



The heterogeneity of the lipid distribution in biomembranes plays a variety of important roles in various physiological phenomena. The lipid domains enriched with sphingolipids and cholesterol, called lipid rafts, have been attracting substantial attention over the past decade.<sup>1,2</sup> However, the small size (10–200 nm)<sup>3</sup> and heterogeneity of lipid rafts have hindered their detailed characterization by conventional optical microscopy.

Mixtures of sphingolipids and cholesterol form a characteristic liquid-ordered phase in which the acyl chains of lipids are ordered and mostly extended, and at the same time the lipid molecules have a high rotational and lateral mobility.<sup>4–6</sup> The liquid-ordered domain is segregated from the surrounding liquid-disordered membrane, where the acyl chains are highly mobile and the molecules undergo fast rotational and lateral diffusion.<sup>7</sup> Liquid-ordered domains can be reconstituted by using model membranes such as monolayers, liposomes, and supported bilayers of relatively simple lipid composition. These model membranes have been extensively investigated with various techniques.<sup>8,9</sup> However, the localization of lipid itself in the membrane is not easily identified mainly because of the lack of appropriate methods.

Atomic force microscopy (AFM) of the supported lipid monolayer or bilayer provides nanometer-scale information as a map of membrane thickness, enabling us to identify the lipid phase.<sup>7,10–12</sup> The advantage of AFM is that it does not require molecular labeling or fixation with the resolution covering from the molecular scale to hundreds of micrometers within aqueous environment. Since bilayers in the solid or liquid-ordered phase

are thicker than bilayers in liquid or liquid-disordered phase, the height image of AFM gives the information on the size and distribution of sphingolipid or sphingolipid/cholesterol domains in phospholipid membrane. AFM clearly shows that the addition of cholesterol increases the size of sphingomyelin (SM) domains in fluid phosphatidylcholine (PC) membranes.<sup>13,14</sup> AFM has also revealed that the degree of unsaturation of the fatty acid in fluid PC phase affects the degree of phase separation of SM and PC.<sup>15</sup> The solubilization of specific lipid domains in SM/1,2-dioleoyl-*sn*-glycero-3-phosphocholine (DOPC)/cholesterol membrane by various detergents was also studied by AFM.<sup>16</sup> Combination of AFM and fluorescence correlation spectroscopy revealed the structural and dynamic modification of liquid-ordered domains by ceramide.<sup>17</sup>

Although AFM is highly sensitive to the difference of the height of samples, one drawback of conventional AFM is that it does not detect the chemical identity of the molecules. Thus, the application of AFM to multicomponent membranes has been limited. Covalent binding of the lipid-recognition proteins to the AFM tip and direct force measurement overcomes this drawback.<sup>12,18,19</sup> Peptide–lipid and virus–lipid interactions have been studied using peptide- or virus-conjugated AFM tips.<sup>20,21</sup> It has been shown that, using a glycosylphosphatidylinositol (GPI)-anchored protein specific toxin-conjugated tip,

**Received:** July 28, 2011

**Revised:** December 9, 2011

**Published:** December 9, 2011

GPI-anchored proteins reside within domains were found mechanically stiffer than the surrounding membrane.<sup>22</sup> Using an unmodified tip, the mechanical properties of model bilayers have been studied by measuring the breakthrough force.<sup>23,24</sup> However, localization of specific lipids in bilayer by AFM using lipid-specific protein-conjugated tip has not been achieved yet.

Various kinds of protein toxins have been reported to specifically bind the raft lipids. The B-subunit of cholera toxin binds ganglioside GM1 ( $\text{Gal}\beta 1,3\text{GalNAc}\beta 1,4(\text{NeuAc}\alpha 2,3)\text{Gal}\beta 1,4\text{Glc}\beta 1,1'$ -ceramide) and has long been used as a raft marker.<sup>25,26</sup> Recently, the binding potential between the cholera toxin B pentamer and GM1 was measured by AFM using a toxin-conjugated tip.<sup>27</sup> However, the AFM tip was not used for the purpose of localization of GM1 in phase-separated membrane. Perfringolysin O and other cholesterol-binding toxins have also been employed to label lipid rafts.<sup>28</sup> Sea anemone-derived equinatoxin II preferentially binds SM,<sup>29,30</sup> although the toxin interacts with phosphatidylcholine/cholesterol membrane at low temperature.<sup>31</sup> Perfringolysin O and equinatoxin II have not been used for AFM/force spectroscopy studies.

Lysenin is an earthworm-derived protein toxin that specifically binds SM.<sup>32–34</sup> The binding of the toxin to SM is dependent on the local density of the lipids; i.e., lysenin binds SM only when the lipid forms clusters of 5–6 molecules.<sup>35,36</sup> Thus, lysenin has been used to localize SM clusters both in cells<sup>37–39</sup> and model membranes.<sup>35,40</sup>

In the present study, we produced lysenin-conjugated tips for the purpose of force measurement by AFM. We observed specific binding of the AFM tip to the SM clusters in the supported bilayer. Addition of cholesterol or DOPC to the membrane did not alter the rupture force between membranes and lysenin-grafted tip, whereas these lipids significantly enhanced the extension lengths. Thus, using a lipid-specific probe conjugated AFM tip, it became possible not only to detect the localization of SM clusters but also to measure the mechanical properties of membrane domains with altered local density of SM at the same time.

## MATERIALS AND METHODS

**Materials.** *N*-Palmitoyl-*D*-*erythro*-sphingosylphosphorylcholine (palmitoyl sphingomyelin, PSM) and cholesterol were purchased from Sigma-Aldrich (St. Louis, MO). 1,2-Dipalmitoyl-*sn*-glycero-3-phosphocholine (DPPC) and 1,2-dioleoyl-*sn*-glycero-3-phosphocholine (DOPC) were from Avanti Polar Lipids (Alabaster, AL). Lysenin was from Peptide Institute, Inc. (Osaka, Japan).

**Formation of Supported Lipid Bilayers.** A combination of the Langmuir–Blodgett (LB) and Langmuir–Schaefer (LS) techniques was employed to fabricate the lipid bilayers on mica surfaces. The lipids dissolved in hexane/ethanol (95:5) were deposited at the air/water interface of the Langmuir trough (USI System, Fukuoka, Japan). Milli-Q water was used as the subphase. The solvent was evaporated, and the first LB monolayer was transferred to freshly cleaved mica piece (Ted Pella, Inc., Redding, CA) at a film pressure of 30 mN m<sup>−1</sup> by vertical withdrawal. The mica covered by the first LB monolayer was horizontally brought into contact with the monolayer, which was spread at the surface of the Langmuir trough and compressed to a surface pressure of 30 mN m<sup>−1</sup>. The mica plate covered by lipid bilayers was transferred to buffer solution (10 mM Hepes, 150 mM NaCl, pH 7.3).

**Tip Treatment.** For lysenin conjugation, silicon nitride tips on narrow cantilevers (200 μm long, Digital Instruments, Santa Barbara, CA) were used throughout the experiments. According to a published procedure,<sup>41</sup> the tips were cleaned by sonication in CHCl<sub>3</sub>, UV irradiation ( $\lambda = 185$  and 254 nm) in O<sub>2</sub> flow, and treated in a mixture of 1:2 H<sub>2</sub>O<sub>2</sub> (30%) + H<sub>2</sub>SO<sub>4</sub> at 150 °C for 10 min to form an uniform silicon oxide layer on the surface. This surface, after being dried in air, was ready for the silane-coupling reaction to graft the anchoring groups. The tips were treated in a mildly heated 1% toluene solution of 3-(mercapto)propyltrimethoxysilane (Aldrich Chemicals, Milwaukee, WI) for 10 min to expose the SH groups to the air as described.<sup>42</sup> The functional tips were further treated with bifunctional cross-linker, *N*-succinimidyl pyridyldithiopropionate (SPDP) (Pierce, Rockford, IL), dissolved in 1% ethanol at room temperature for a few hours. The pyridyldithio moiety of SPDP has reactivity toward free SH groups on the tip. A small portion of lysenin solution with a concentration of about 100 μg/mL was applied to the SPDP-terminated tip for a few hours, through the reaction with the free NH<sub>2</sub> groups on the protein molecules toward the *N*-succinimidyl group in another end of SPDP. Finally, the residual intact SPDP was blocked by dipping into a Tris/glycine buffer solution. Since the anchoring moieties (3-(mercapto)propyltrimethoxysilane of which the in-plane molecular diameter is estimated to be less than 1 nm) were abundant, it was assumed that they fully covered the tip surface<sup>42</sup> and were able to accommodate lysenin molecules. To detect the grafted lysenin on the tip surface, the same grafting procedure was performed with lysenin mutant conjugated with red fluorescent protein (RFP),<sup>37</sup> and the tip surface was observed by a fluorescence microscope (Figure 1). The fluorescence was uniformly observed over the silicon nitride of the tip and the body of cantilever.

If a lysenin molecule is properly fixed on the tip surface, we can anticipate a high probability of specific binding of the lysenin molecule to SM in the membrane, judging from the high affinity of lysenin to SM ( $K_D = 5.3 \times 10^{-9}$  M).<sup>32</sup> Our previous study indicates that, among 297 amino acids of lysenin, C-terminal 137 amino acids are required for the binding to SM.<sup>37</sup> However, tryptophan-to-alanine substitution experiment shows that, in addition to tryptophan 245 and 291, tryptophan 20 is also important for the binding of the protein to SM.<sup>43</sup> These results suggest that both binding domain and the higher order structure are important for the binding of lysenin to SM. Thus, in order to bind SM-containing membrane, lysenin has to be properly folded when conjugated to the tip. The lysine residues are the preferential sites for the protein to bind to the anchoring group of tip surface. Lysenin contains 20 lysine residues distributed throughout the protein.<sup>44</sup> Since the crystal structure of lysenin has not been solved yet, it is difficult to predict which lysine residue is involved in the linkage of the protein to the surface. One can speculate that the binding of lysenin to the tip via lysine residue would change the higher order structure and inhibit the activity of the protein. Indeed, not all lysenin-conjugated tips exhibited binding to SM-containing supported bilayers.

AFM height imaging was performed using plain tips without lysenin conjugation.

**AFM Measurement.** Nanoscope III multiprobe AFM (Digital Instruments, Santa Barbara, CA) with a J-scanner was used in the force measurements. The calibration of spring constant of each modified cantilever was performed in solution by a method based on the measurement of the thermal

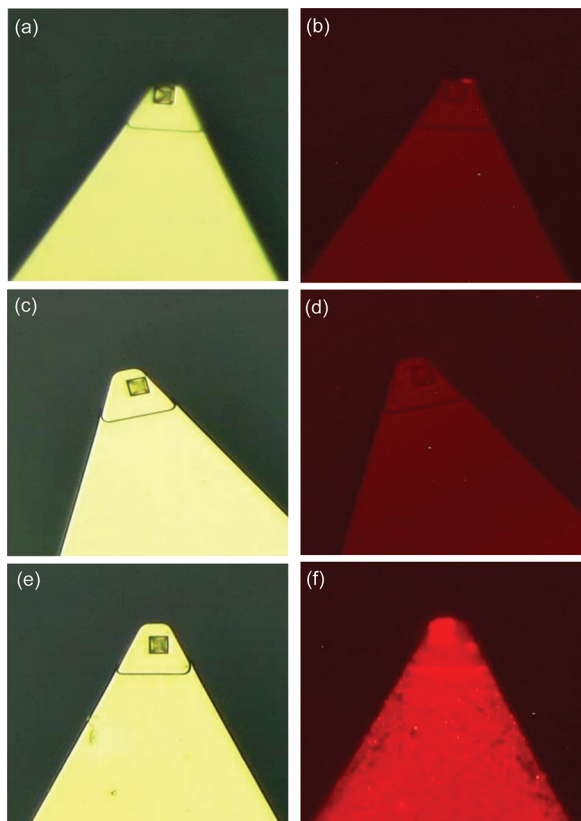


**Figure 1.** Optical microscopic images of an AFM tip/cantilever assembly before and after conjugation of lysenin to the surface. (a, b) The AFM tip was treated with 3-(mercaptopropyl)trimethoxysilane. (c, d) The tip in (a, b) was further treated with bifunctional cross-linker, *N*-succinimidyl pyridyldithiopropionate (SPDP). (e, f) The tip in (c, d) was further treated in the solution of RFP-lysenin. (a, c, e) Bright field image. (b, d, f) Fluorescence image.

vibrations as described previously.<sup>45</sup> The typical spring constant was  $\sim 50$  pN/nm of cantilever bending. A substrate with supported lipid membrane was mounted on the AFM sample stage, and a liquid cell was constructed over it. Force curves were obtained in 10 mM Hepes, 150 mM NaCl, pH 7.3, at room temperature by modulating the z-axis-directed piezo motion. The relative trigger mode was used to keep the tip-loading force below 300 pN to minimize the damage to the lipid membrane directly under the tip. We adjusted the z-axis scanning speed from 250 to 500 nm s<sup>-1</sup> for both approaching and withdrawing.

## RESULTS AND DISCUSSION

The AFM force curve usually varies run by run because of the uncontrollable microscopic status of the surfaces of tip and sample. Thus, we repeated recording force curves in order to obtain essential force parameters statistically. Although we tried to keep the tip-loading force condition equal for each run, we could not observe any attractive force in most of the runs. The frequency of nonadhesive approach was larger than 90% for all the examined bilayers containing PSM.

The second frequent case was that a single peak of attractive force was measured in the tip retracting action. This sort of force curve is considered to represent a mechanical event between a single lysenin molecule and SM in the bilayer. Figures 2a,c show such force curves obtained on (a) PSM bilayer and (c) 1:1 PSM + DOPC bilayer. Finite negative

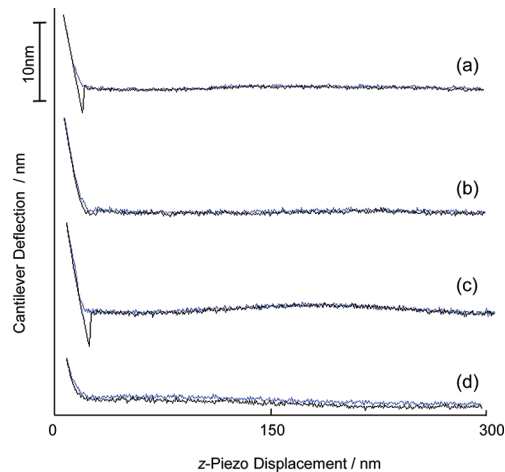


**Figure 2.** Typical raw force curves, represented as z-piezo displacement/nm versus cantilever deflection/nm, of the tip-conjugated lysenin to different membranes. Blue lines indicate approaching curves whereas black lines show retraction curves. The force constants of cantilevers used were 50 pN nm<sup>-1</sup> in average, and the scanning speed for z-piezo displacement was 500 nm s<sup>-1</sup> both for approaching and retracting (loading rate in approach = 2500 pN s<sup>-1</sup>). (a) A typical force curve obtained with lysenin-attached tip on a bilayer of *N*-palmitoyl-*D*-erythro-sphingosylphosphorylcholine (PSM). Loading force = 300 pN. (b) A force curve on a bilayer of 1,2-dipalmitoyl-sn-glycero-3-phosphocholine (DPPC). Loading force = 300 pN. (c) A force curve with lysenin-attached tip on a PSM/1,2-dioleoyl-sn-glycero-3-phosphocholine (DOPC) (1:1) bilayer. Loading force = 400 pN. (d) A force curve with lysenin-attached tip on a bilayer of PSM/DPPC (1:1). Loading force = 200 pN.

(attractive) peaks were observed on the force curve, indicating the interaction of the lysenin-conjugated tip with the bilayer. We did not detect any attractive force peak on DPPC bilayers, although we recorded more than 300 force curves while changing the tip. Figure 2b shows a representative force curve on pure DPPC bilayers. The absence of attractive force for pure DPPC is a distinctive difference from PSM-containing bilayers. Our results indicate the specific interaction of the lysenin-conjugated tip with PSM. This result also indicates that at least a part of lysenin molecules retains its activity after the conjugation to the AFM tip.

In the case of (d) PSM + DPPC, attractive interaction was seldom seen. Lysenin did not bind PSM in PSM + DPPC bilayer in this case. This is in an agreement with the nature of the interaction of lysenin and SM-containing bilayer. A characteristic feature of lysenin is that this protein binds to SM only when the local concentration of SM is high.<sup>34,35,46</sup> Isothermal calorimetry indicates the binding stoichiometry of lysenin:SM is 1:5, suggesting that one lysenin molecule binds a lipid cluster containing five SM molecules.<sup>35</sup> At room temperature, PSM and DPPC are in a gel state, whereas DOPC is a liquid crystalline. It has been reported that DOPC is hardly miscible with SM,<sup>47</sup> whereas DPPC and SM are completely miscible.<sup>48</sup> Thus, SM molecules form clusters in DOPC but not in DPPC membranes.<sup>35</sup> The results of the present fishing curves are consistent with our previous biochemical observation.<sup>35</sup>

Within the range from 100 to 300 pN of the loading force, and the range from 250 to 500 nm s<sup>-1</sup> (approximately 1250–2500 pN s<sup>-1</sup>) of the z-scan rate, we experienced no systematic changes in the single-peak force curves. The experiments were

performed at room temperature after the thermal drifting was settled for all the solutions and components of the AFM to be used in the experiment. The frequency of force detection significantly decreased after 1000 runs. In that case, we changed the tip and started measurement again. This tip deterioration might be due to loss of the active lysenin molecules on the tip apex or contamination of lipids around the active lysenin molecule. To obtain 100 successful plots, we had to exchange the tip to new one twice or three times. The average values of peak force were not significantly different between the beginning and the end of the measurement. Therefore, we believe that as long as we used new tips, we did not see biased results anticipated from contamination.

Figure 3a schematically illustrates the AFM force–distance cycles. The “fishing” process starts from approaching of the tip to the sample in the buffer solution. When the tip touches the sample, a repulsive force is observed. We limited this force lower than the preset value (step 1) below 300 pN to reduce the probability of destroying the tip/sample surfaces and multiple-point interactions. Then, the tip is retracted, and an increasing adhesive force is started to be observed at point X. This is the pulling-out process of a PSM cluster bound with a lysenin molecule on the tip. At a certain level of adhesive force, the molecular connection breaks (step 2) and the force between the tip and sample returns to the zero level (step 3). This “fishing” process in the force measurement is characteristic to the binding of protein on the tip and lipid on the substrate.

Since the force curves on each of the bilayers varied run by run, it was necessary to handle the results statistically. We used two representative parameters describing the attractive peak on the force curve, that is, the peak extension ( $d/\text{nm}$ ) and the peak force ( $f/\text{pN}$ ). These numbers are obtained on genuine force curves, which are processed from the raw force curves by reducing the effect of cantilever deflection. This process is described in detail in ref 49. In the present case, the raw force curve ( $Z$ -piezo displacement  $Z/\text{nm}$  versus cantilever deflection  $\delta/\text{nm}$ ) was converted into tip–substrate distance  $H/\text{nm}$  versus force  $F/\text{pN}$ , using

$$H = Z + \delta - H_0, \quad F = k\delta \quad (1)$$

where  $k$  denotes the spring constant of cantilever, and  $H_0$  is the  $H$  offset, defined as the  $Z$ -value at point  $X$  in Figure 3a. Figure 3b illustrates the  $H$ – $F$  curve.  $H$  represents the true elongation of molecular entities between the tip and the substrate. The peak extension  $d$  is given as the distance of the negative peak position from the zero-cross point of the  $F$ – $H$  curve. The peak force  $f$  is the depth of negative peak. All the raw force curves were numerically converted into  $H$ – $F$  curves, and the pairs of  $d$  and  $f$  were calculated.

Much less frequently, we observed multiple attractive force peaks. Such cases are associated with multipoint interaction with lysenin molecules and the lipid bilayer, which are excluded from our data statistics.

Figures 4a,c,e show typical AFM height images for PSM and PSM + cholesterol mixed bilayers. The dark (reddish-brown) area in Figures 4a,c,e is assigned to the bare mica substrate, judged from the heights of hole edges ( $\approx 5 \text{ nm}$ ) resembling the thickness of lipid bilayer. To avoid damaging, we did not perform scanning for imaging using lysenin conjugated tips before force curve measurement on the same sample surface. We could not specify the in-plane position of force curve recording on the bilayer. Thus, the lysenin-conjugated tip sometimes approached to the space where the membranes were

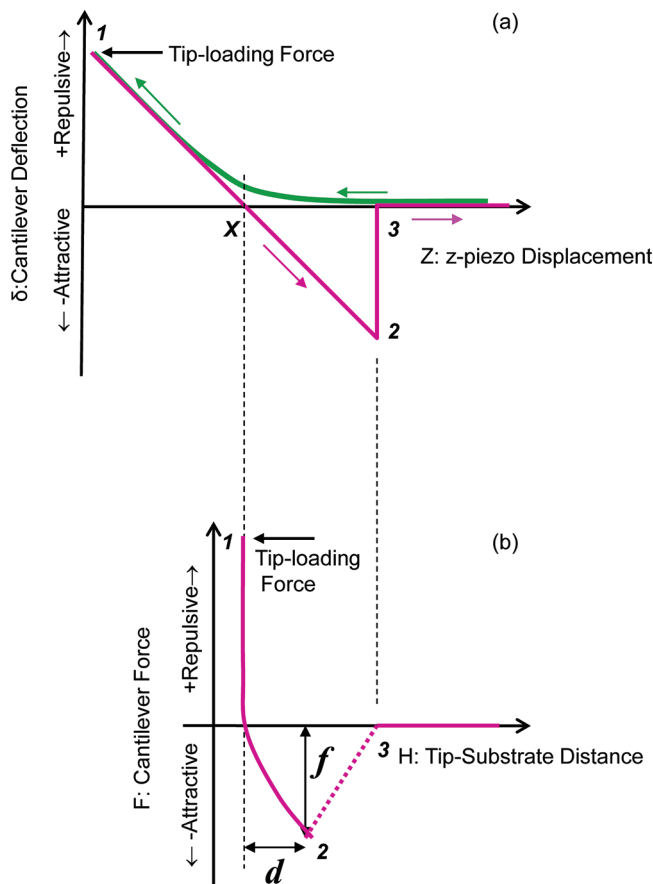


**Figure 3.** Schematic representation of an AFM force–distance cycle with lysenin-attached tip on sphingomyelin (SM)-containing membrane. Frame (a) schematizes the raw force curves, indicating the cantilever deflection ( $\delta/\text{nm}$ ) as a function of  $z$ -piezo displacement ( $Z/\text{nm}$ ). The tip was moved toward the membrane surface (on green line, toward point 1) and subsequently retracted (pink line, toward point 2) with the in-plane tip position fixed. During tip approach, lysenin binds to SM, leading to a force signal with a distinct shape (point 1 to point 2) while the tip is retracted. The force increases until the dissociation occurs (from point 1 to point 2). The raw force curves were numerically converted by eq 1 in the text into the force ( $F/\text{pN}$ ) as a function of the tip–substrate distance ( $H/\text{nm}$ ), shown in frame (b). When the dissociation occurs (point 2), the cantilever returns to the neutral position and the tip travels back to point 3 by the distance of deflection. The negative peak at point 2 provides two characteristic parameters, that is, the peak extension ( $d/\text{nm}$ ) and the peak force ( $f/\text{pN}$ ). The peak extension is given as the distance of the negative peak position from the zero-cross point ( $X$ ) of the  $F$ – $H$  curve. The peak force is the depth of negative peak.

not attached, resulting in reducing the overall probability of lysenin–SM binding.

Figures 4b,d,f are the scattering plots of  $(d, f)$  pairs over the peak-force/peak-extension plane, calculated from the force curves. Figure 4b shows the binding of lysenin-conjugated tip to the PSM bilayer. Most of the points are concentrated at a small peak extension centered at  $\bar{d} = 0.6 \pm 1.6 \text{ nm}$ . The peak-force scatters in the range of  $\bar{f} = 182 \pm 53 \text{ pN}$  (see also Figure 7). These results demonstrate that the extension of lysenin molecule on the tip as well as on the pure PSM bilayer was minimal, indicating that this lysenin/bilayer assembly was rigid and dissociated with an extension of a few tenths of the PSM molecular length ( $\approx 2.5 \text{ nm}$ ). It is notable that the lysenin molecules were not brought into the form of an extended

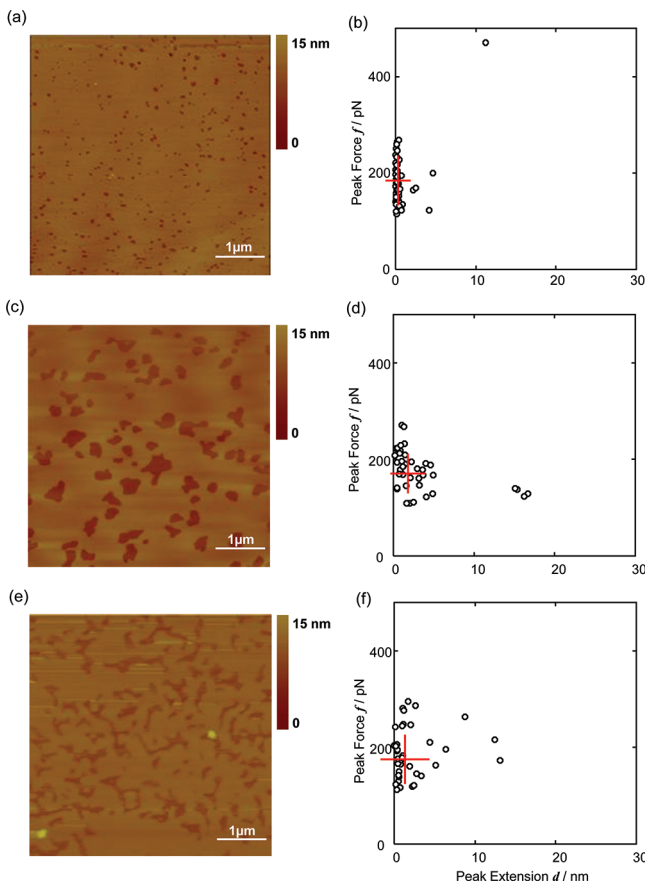


**Figure 4.** AFM contact-mode height image with untreated tips and the scattering plots for the peak force  $f$  and peak extension  $d$  between lysenin-conjugated tips and pure PSM or PSM/cholesterol bilayer on mica. The loading force and loading speed for force measurement were fixed at 300 pN and 500 nm s<sup>-1</sup>, respectively. (a, b) For pure PSM. The scattering plot contains 63 points. The averages,  $\bar{f} = 182 \pm 53$  pN and  $\bar{d} = 0.6 \pm 1.6$  nm, are indicated by a cross in the plane. (c, d) 85:15 PSM + cholesterol, 39 points,  $\bar{f} = 176 \pm 41$  pN and  $\bar{d} = 3.4 \pm 4.4$  nm. (e, f) 67:33 PSM + cholesterol, 39 points,  $\bar{f} = 188 \pm 51$  pN and  $\bar{d} = 2.2 \pm 3.1$  nm.

peptide chain. This is also evident in the raw force curves, in which the  $Z$  region for dragging a loose protein chain is missing<sup>49</sup> below point “X” in Figure 3a. The lysenin molecules could become rigid because of multipoint binding with the tip surface. The small variation of peak force may be associated with the various orientation of lysenin molecules fixed on the tip surface.

Figures 4d,f indicate that the addition of cholesterol to PSM did not significantly alter the distribution of  $f$ . The distribution of  $d$  was centered at a few nanometers in the presence of cholesterol. This value is close to a full extended length of one PSM molecule. These results suggest that the addition of cholesterol did not change the lysenin–PSM binding force but increased the vertical mobility of the PSM molecules. The observation that cholesterol did not alter the peak force is consistent with our previous result that the addition of cholesterol to SM liposomes did not affect the binding of lysenin to SM.<sup>36</sup>

Figure 5 shows an AFM image and the scattering plot for 1:1 PSM/DOPC bilayer. AFM height image indicates the formation of PSM-rich higher small domains in DOPC-rich lower membrane, as previously reported.<sup>14</sup> The height

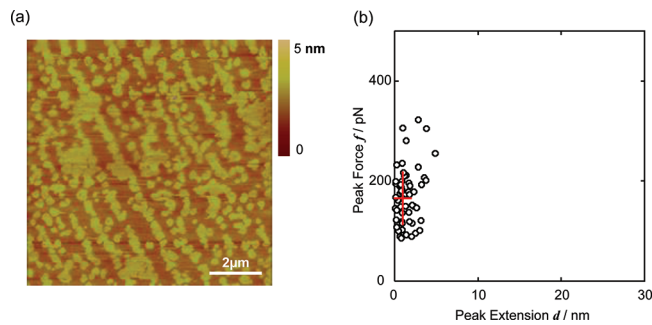


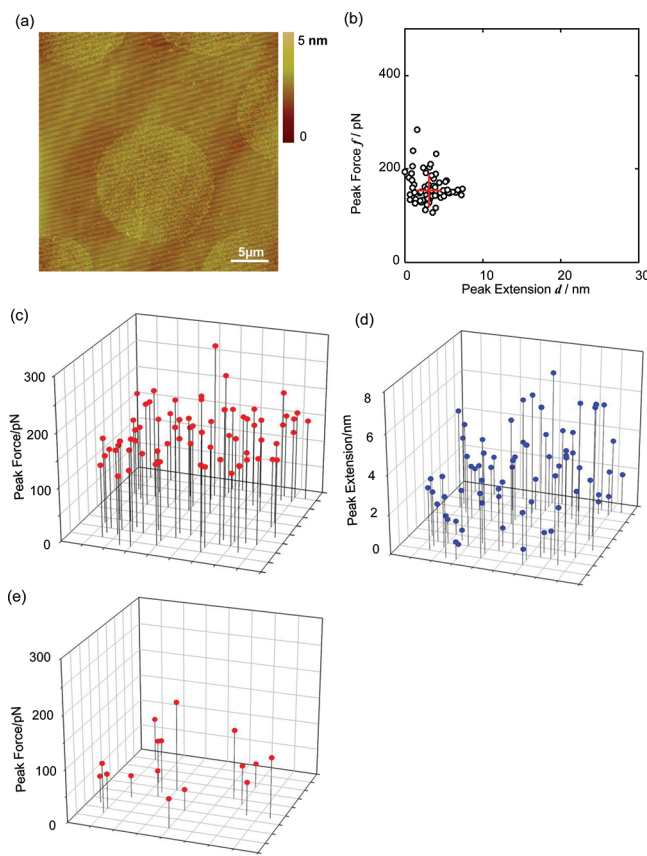
**Figure 5.** AFM contact-mode height image with untreated tips (a) and the scattering plot for the peak force and peak extension between a lysenin-conjugated tip and a binary-mixture bilayer of 1:1 PSM + DOPC on mica (b). The loading force and loading speed for force measurement were fixed at 300 pN and 500 nm s<sup>-1</sup>, respectively. This plot is composed of 61 points, and the average values are  $\bar{f} = 172 \pm 54$  pN and  $\bar{d} = 1.5 \pm 1.1$  nm, indicated by the cross.

difference between bright (yellowish) area and dark (brownish) area was about 1.6 nm. The scattering plots of (d, f) pairs are shown in Figure 5b. Figures 5b and 7 indicate that, similar to PSM/cholesterol bilayer, the affinity of lysenin to PSM represented by the peak force was not significantly altered by the presence of DOPC. The peak extension is apparently longer than that of pure PSM but shorter than those of cholesterol-containing membranes.

Figure 6 shows AFM height images of PSM/DOPC 1:1 mixture containing 15% cholesterol (PSM:DOPC:cholesterol = 42.5:42.5:15). In Figure 6a, circular wrinkled zones with diameters  $\sim 10$  μm were recognized. The height difference between the circular zone and the complementary zone was about 1.3 nm. We used a macro program for AFM to map the peak force and the peak extension in and out of the circular wrinkled domains. This macro places the tip on the pixels within a finite square area. For each pixel point within the square, the macro fixes the in-plane position of tip and makes an approach scan up to the given repulsive loading force. Then a retraction scan is made, with the force recorded as a function of the tip–sample distance. After the scan is completed, the macro judges whether a significant single attractive force peak is observed or not. This judgment is made by comparing the maximum attractive force on the curve with a given level ( $f < 20$  pN). If the curve is always below the level, the same cycle is repeated at the same in-plane position. If an attractive single force peak is observed, then the values of peak force  $f$  and peak extension  $d$  are associated with the position of pixel, and the tip is moved to the next pixel. If no attractive peak larger than 20 pN is recognized after 100 times of tip retraction, then the values of  $f$  and  $d$  are recorded as void, and the tip is moved to the next pixel.

To position the AFM tip in and out of the circular wrinkled zones, an optical microscope integrated in the AFM setup was utilized. The positions of circular zones were subtly visible in the microscopic view. This procedure was taken to avoid damaging the lysenin-conjugated tips.

Figures 6c–e show the distribution of  $f$  and  $d$  over the scanned area, in and out of the circular wrinkled zone. The peak force in the circular wrinkled zone (Figure 6c) was constantly around 160 pN (also Figures 6b and 7), suggesting lysenin–PSM binding in this zone. Figure 6d shows the spatial distribution of peak extension in the same area. The average of the peak extensions was about 3 nm (also Figures 6b and 7).



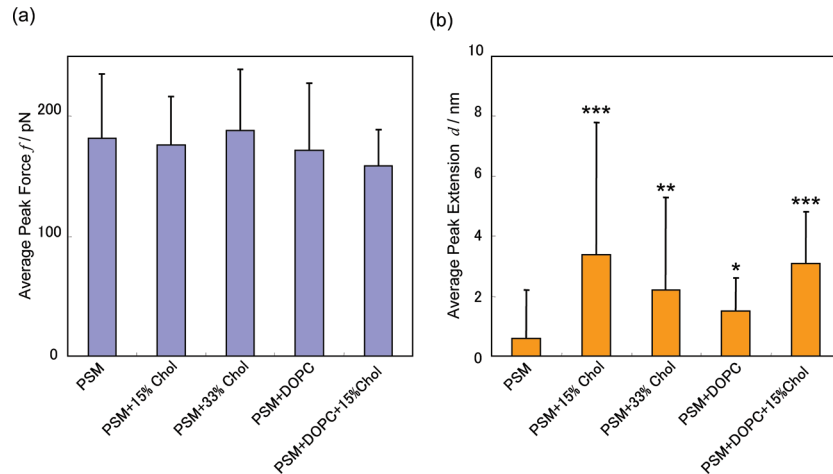
**Figure 6.** AFM contact-mode height image (a) and the distribution of the peak force/peak extension between lysenin and the ternary mixed PSM/DOPC/cholesterol (42.5:42.5:15) bilayer. (b) The scattering plot for the peak force and peak extension. 71 points,  $\bar{f} = 157 \pm 34$  pN and  $\bar{d} = 3.08 \pm 1.78$  nm. The loading force and loading speed for force measurement were fixed at 300 pN and 500 nm s<sup>-1</sup>, respectively. (c) Two-dimensional distribution of binding force for the SM-rich area ( $2 \mu\text{m} \times 2 \mu\text{m}$  divided into 81 ( $9 \times 9$ ) points) were selected for force recording. (d) Two-dimensional distribution of peak extension for the same area. (e) Two-dimensional distribution of binding force recorded in SM-poor area. The force mapping was operated in a  $2 \mu\text{m} \times 2 \mu\text{m}$  square area, divided into 72 ( $8 \times 9$ ) points. Initial loading force = 300 pN. The points where the peak force was less than 20 pN were not plotted.

Figure 6e indicates the two-dimensional distribution of the peak force outside the circular wrinkled zones. The peak force was of the zero level at most of data points. These results indicate that we could distinguish PSM-rich areas and PSM-poor areas in a bilayer by combining AFM imaging and force mapping using lysenin-conjugated tip. Figure 6b shows the scattering plots obtained for the same PSM + DOPC + cholesterol mixed bilayer. As mentioned above, the zero-peak-force curves were all omitted from the statistics, and thus the PSM-poor zone was automatically excluded.

Figure 7 summarizes the average values of peak force and peak extension obtained in Figures 4–6. The force for lysenin–PSM adhesion was essentially constant and equal to a value close to 170 pN, judged from the variation of peak force. In all of the scattering plots, there was no clear relationship between the peak force and peak extension. When lysenin-conjugated tip bound the membrane, the peak force was not dependent on the lipid composition of the bilayer under our experimental conditions. The adhesion force of the bilayer to the substrate measured by AFM was reported to be higher than a few nN,<sup>23,50,51</sup> which is 5–10 times higher than the peak force observed in this study. Thus, it is unlikely that the lysenin tip detaches the bulk bilayer from the mica in our experimental condition. We obtained adhesion force of lysenin and SM around 170 pN. Since one lysenin molecule binds five SM molecules,<sup>35</sup> the adhesion force of lysenin to one SM is calculated to be 34 pN. This value is close to the adhesion force of cholera toxin and ganglioside GM1 (50–60 pN).<sup>27</sup>

The peak extensions of the PSM + cholesterol mixed bilayers, the PSM + DOPC mixed bilayer, and the PSM + DOPC + cholesterol ternary mixed bilayer are definitely different from that of the pure PSM bilayer. To evaluate the peak extension values, all the plots were subjected to statistical Student's *t* test. The matching probability of the mixed bilayers with pure PSM bilayers are plotted by the number of stars. The addition of both cholesterol and DOPC significantly increased the average peak extension. In most cases, the plotted peak extensions were within the full length of one phospholipid molecule ( $\approx 2.5$  nm).

We anticipate that the peak extension values summarized in Figure 7 originate from the deformation of the membrane pulled up by the lysenin-conjugated tip. Our results suggest that



**Figure 7.** Summary for the average values of (a) peak force and (b) peak extension for the PSM-containing bilayers in Figures 4–6. In (b), the matching probability  $P$  with the pure PSM bilayer, calculated by Student's *t* test, are indicated as follows: \*,  $P < 0.01$ ; \*\*,  $P < 0.002$ ; \*\*\*,  $P < 0.001$ .

the degree of deformation depends on the lipid composition of the leaflet. The gel to liquid crystalline phase transition temperature of PSM is 41 °C.<sup>48,52</sup> Thus, PSM bilayer was in gel phase during our AFM measurement at room temperature. The effect of cholesterol on mechanical properties of gel phase lipid (dimyristoylphosphatidylcholine, DMPC, at 15 °C) has been examined by micropipet pressurization of giant single-walled vesicles.<sup>53</sup> Addition of 12.5% cholesterol significantly increased thermal area expansivity (from 1.0 to 2.83). This value was decreased to 1.97 when cholesterol was increased to 33%. In our system, average peak extension was increased by the addition of 15% cholesterol to PSM ( $0.6 \pm 1.6$  to  $3.4 \pm 4.4$  nm), and it was decreased to  $2.2 \pm 3.1$  nm in the presence of 33% cholesterol. These results are consistent with the results of Needham et al.,<sup>53</sup> who also showed that liquid crystalline membrane exhibits higher thermal area expansivity than gel phase lipid. In our experiment, the addition of DOPC increased the average peak extension of PSM. The thermogram of equimolar mixture of DOPC and PSM shows lower phase transition temperature of PSM-rich phase, indicating the partial mixing of DOPC to PSM.<sup>54</sup> The mixing of DOPC explains the increase of average peak extension of PSM.

Figure 8 schematizes our results on the interaction of various supported bilayers with lysenin-conjugated tip. The pure DPPC bilayer exhibits no specific interaction with lysenin, and no attractive force is observed (Figure 8a). Figure 8b is the case for pure PSM bilayer. When the PSM cluster is captured and pulled out by lysenin, the hydrophobic part can be exposed to water, resulting in a strong pulling-back force. In the case of mixed bilayers (Figure 8c), DOPC and cholesterol molecules surrounding the PSM cluster can also be pulled up, reducing the effect of hydrophobic force. This represents the elasticity of lipid membrane depending on the bilayer composition. Occasionally, plots with long peak extensions (>10 nm) were observed. Such plots were still with peak forces within the range around 170 pN. This can be attributed to the unfolding of lysenin molecules on the tip surface.

Because of the clear difference in the peak force, we can distinguish PSM containing bilayers from PSM free bilayers. Our method of conjugating AFM with a protein that recognizes specific lipid provides a promising means for investigating the localization and mechanical properties of specific lipid domains. We expect that the application of this AFM/force measurement for the outer surfaces of live cells will be useful in gaining deep insights for the dynamic action of cell membranes at the nanoscopic scale.

## CONCLUSION

Using the lysenin-conjugated AFM tips, we could successfully obtain the statistics of mechanical properties (peak force  $f$  and peak extension  $d$ ) of pure and mixed PSM bilayers.

(1) The specificity of lysenin binding with PSM domains was demonstrated. The PSM bilayer and PSM mixed with liquid phase DOPC exhibited finite peak force. On the other hand, bilayers without PSM and PSM mixed with gel phase DPPC exhibited zero peak force.

(2) The average peak force between lysenin and PSM-including bilayers was in the range 150–190 pN and was independent of whether the PSM alone or mixed with DOPC or cholesterol. The peak force represents the binding between a lysenin molecule and a PSM cluster.

(3) The peak extension varied depending on the composition of lipid bilayer. For pure PSM bilayer the peak

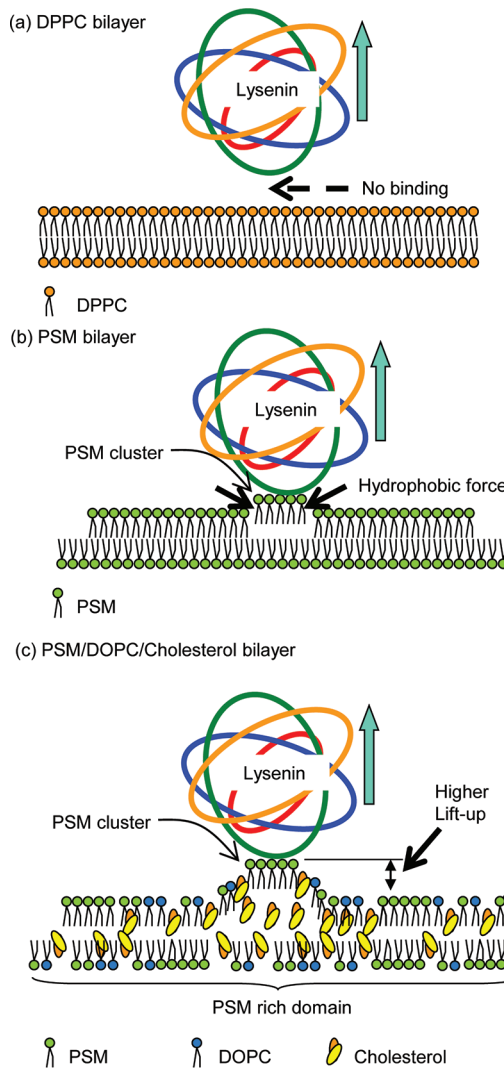


**Figure 8.** Schematic illustration for PSM cluster sliding motion upon attachment to lysenin and lifting up motion: (a) pure DPPC bilayer, (b) pure PSM bilayer, (c) PSM + DOPC + cholesterol bilayer.

extension was the minimum. Cholesterol and DOPC enhance the integrity of lipid bilayers by increasing the apparent mechanical elasticity.

(4) By mapping the force curves two-dimensionally, we were able to distinguish PSM-rich and PSM-poor domains in AFM images.

## AUTHOR INFORMATION

### Corresponding Author

\*Tel: +81-48-467-9534. Fax: +81-48-467-9535. E-mail: tayamada@riken.jp (T.Y.); kobayasi@riken.jp (T.K.).

### Present Address

<sup>†</sup>Biomedical Systems Japan G.K., Tsukuba, Ibaraki 305-0817, Japan.

### Funding

This study was supported in part by RIKEN President Discretionary Fund (2004–2006, 2010–2012) (M.H., T.Y., and T.K.), Lipid Dynamics Program of RIKEN (T.Y. and T.K.), Grants-in-Aid for Scientific Research on Promotion of Novel Interdisciplinary Fields Based on Nanotechnology and Materials, and Grants-in-Aid for Scientific Research 22390018

(to T.K.) from the Ministry of Education, Culture, Sports, Science and Technology of Japan.

## ACKNOWLEDGMENTS

We are grateful to Motohide Murate, Reiko Ishitsuka, Takuma Kishimoto, and Françoise Hullin-Matsuda for critically reading the manuscript.

## ABBREVIATIONS

AFM, atomic force microscopy; DPPC, 1,2-dipalmitoyl-sn-glycero-3-phosphocholine; DOPC, 1,2-dioleoyl-sn-glycero-3-phosphocholine; GPI, glycosylphosphatidylinositol; LB, Langmuir-Blodgett; LS, Langmuir-Schaefer; PSM, N-palmitoyl-D-erythro-sphingosylphosphorylcholine; SM, sphingomyelin; SPDP, N-succinimidyl pyridyldithiopropionate.

## REFERENCES

- (1) Lingwood, D., and Simons, K. (2010) Lipid Rafts As a Membrane-Organizing Principle. *Science* 327, 46–50.
- (2) Jacobson, K., Mouritsen, O. G., and Anderson, R. G. (2007) Lipid rafts: at a crossroad between cell biology and physics. *Nat. Cell Biol.* 9, 7–14.
- (3) Pike, L. J. (2006) Rafts defined: a report on the Keystone Symposium on Lipid Rafts and Cell Function. *J. Lipid Res.* 47, 1597–1598.
- (4) Edidin, M. (2003) The state of lipid rafts: from model membranes to cells. *Annu. Rev. Biophys. Biomol. Struct.* 32, 257–283.
- (5) London, E. (2005) How principles of domain formation in model membranes may explain ambiguities concerning lipid raft formation in cells. *Biochim. Biophys. Acta* 1746, 203–220.
- (6) Garcia-Saez, A. J., and Schwille, P. (2010) Stability of lipid domains. *FEBS Lett.* 584, 1653–1658.
- (7) Giocondi, M. C., Yamamoto, D., Lesniewska, E., Milhiet, P. E., Ando, T., and Le Grimellec, C. (2010) Surface topography of membrane domains. *Biochim. Biophys. Acta* 1798, 703–718.
- (8) Lagerholm, B. C., Weinreb, G. E., Jacobson, K., and Thompson, N. L. (2005) Detecting microdomains in intact cell membranes. *Annu. Rev. Phys. Chem.* 56, 309–336.
- (9) Garcia-Saez, A. J., and Schwille, P. (2010) Surface analysis of membrane dynamics. *Biochim. Biophys. Acta* 1798, 766–776.
- (10) Johnston, L. J. (2007) Nanoscale imaging of domains in supported lipid membranes. *Langmuir* 23, 5886–5895.
- (11) Frederix, P. L., Bosshart, P. D., and Engel, A. (2009) Atomic force microscopy of biological membranes. *Biophys. J.* 96, 329–338.
- (12) Goksu, E. I., Vanegas, J. M., Blanchette, C. D., Lin, W. C., and Longo, M. L. (2009) AFM for structure and dynamics of biomembranes. *Biochim. Biophys. Acta* 1788, 254–266.
- (13) Rinia, H. A., Snel, M. M., van der Eerden, J. P., and de Kruijff, B. (2001) Visualizing detergent resistant domains in model membranes with atomic force microscopy. *FEBS Lett.* 501, 92–96.
- (14) Lawrence, J. C., Saslowsky, D. E., Edwardson, J. M., and Henderson, R. M. (2003) Real-time analysis of the effects of cholesterol on lipid raft behavior using atomic force microscopy. *Biophys. J.* 84, 1827–1832.
- (15) Shaikh, S. R., Damaula, A. C., Castillo, A., LoCascio, D., Siddiqui, R. A., Stillwell, W., and Wassall, S. R. (2004) Oleic and docosahexaenoic acid differently phase separate from lipid raft molecules: a comparative NMR, DSC, AFM, and detergent extraction study. *Biophys. J.* 87, 1752–1766.
- (16) Garner, A. E., Smith, D. A., and Hooper, N. M. (2008) Visualization of detergent solubilization of membranes: implications for the isolation of rafts. *Biophys. J.* 94, 1326–1340.
- (17) Chiantia, S., Kahya, N., Ries, J., and Schwille, P. (2006) Effects of ceramide on liquid-ordered domains investigated by simultaneous AFM and FCS. *Biophys. J.* 90, 4500–4508.
- (18) Hinterdorfer, P., and Dufrene, Y. F. (2006) Detection and localization of single molecular recognition events using atomic force microscopy. *Nature Methods* 3, 347–355.
- (19) Muller, D. J. (2008) AFM: a nanotool in membrane biology. *Biochemistry* 47, 7986–7998.
- (20) Andre, G., Brasseur, R., and Dufrene, Y. F. (2007) Probing the interaction forces between hydrophobic peptides and supported lipid bilayers using AFM. *J. Mol. Recognit.* 20, 538–545.
- (21) Carneiro, F. A., Lapido-Loureiro, P. A., Cordo, S. M., Stauffer, F., Weissmuller, G., Bianconi, M. L., Juliano, M. A., Juliano, L., Bisch, P. M., and Da Poian, A. T. (2006) Probing the interaction between vesicular stomatitis virus and phosphatidylserine. *Eur. Biophys. J.* 35, 145–154.
- (22) Roduit, C., van der Goot, F. G., De Los Rios, P., Yersin, A., Steiner, P., Dietler, G., Catsicas, S., Lafont, F., and Kasas, S. (2008) Elastic membrane heterogeneity of living cells revealed by stiff nanoscale membrane domains. *Biophys. J.* 94, 1521–1532.
- (23) Sullan, R. M., Li, J. K., and Zou, S. (2009) Direct correlation of structures and nanomechanical properties of multicomponent lipid bilayers. *Langmuir* 25, 7471–7477.
- (24) An, H., Nussio, M. R., Huson, M. G., Voelcker, N. H., and Shapter, J. G. (2010) Material properties of lipid microdomains: force-volume imaging study of the effect of cholesterol on lipid microdomain rigidity. *Biophys. J.* 99, 834–844.
- (25) Lencer, W. I., and Saslowsky, D. (2005) Raft trafficking of ABS subunit bacterial toxins. *Biochim. Biophys. Acta* 1746, 314–321.
- (26) Ishitsuka, R., and Kobayashi, T. (2008) The use of lipid-binding toxins to study the distribution and dynamics of sphingolipids and cholesterol, in *Probes and Tags to Study Biomolecular Function* (Miller, L. W., Ed.) pp 53–71, Wiley-VCH, Weinheim.
- (27) Cai, X. E., and Yang, J. (2003) The binding potential between the cholera toxin B-oligomer and its receptor. *Biochemistry* 42, 4028–4034.
- (28) Ohno-Iwashita, Y., Shimada, Y., Hayashi, M., Iwamoto, M., Iwashita, S., and Inomata, M. (2010) Cholesterol-binding toxins and anti-cholesterol antibodies as structural probes for cholesterol localization. *Subcell Biochem.* 51, 597–621.
- (29) Bakrac, B., Gutierrez-Aguirre, I., Podlesek, Z., Sonnen, A. F., Gilbert, R. J., Macek, P., Lakey, J. H., and Anderluh, G. (2008) Molecular determinants of sphingomyelin specificity of a eukaryotic pore-forming toxin. *J. Biol. Chem.* 283, 18665–18677.
- (30) Bakrac, B., Kladnik, A., Macek, P., McHaffie, G., Werner, A., Lakey, J. H., and Anderluh, G. (2010) A toxin-based probe reveals cytoplasmic exposure of Golgi sphingomyelin. *J. Biol. Chem.* 285, 22186–221895.
- (31) Caaveiro, J. M., Echabe, I., Gutierrez-Aguirre, I., Nieva, J. L., Arrondo, J. L., and Gonzalez-Manas, J. M. (2001) Differential interaction of equinatoxin II with model membranes in response to lipid composition. *Biophys. J.* 80, 1343–1353.
- (32) Yamaji, A., Sekizawa, Y., Emoto, K., Sakuraba, H., Inoue, K., Kobayashi, H., and Umeda, M. (1998) Lysenin, a novel sphingomyelin-specific binding protein. *J. Biol. Chem.* 273, 5300–5306.
- (33) Shakor, A. B., Czurylo, E. A., and Sobota, A. (2003) Lysenin, a unique sphingomyelin-binding protein. *FEBS Lett.* 542, 1–6.
- (34) Shogomori, H., and Kobayashi, T. (2008) Lysenin: A sphingomyelin specific pore-forming toxin. *Biochim. Biophys. Acta* 1780, 612–618.
- (35) Ishitsuka, R., Yamaji-Hasegawa, A., Makino, A., Hirabayashi, Y., and Kobayashi, T. (2004) A lipid-specific toxin reveals heterogeneity of sphingomyelin-containing membranes. *Biophys. J.* 86, 296–307.
- (36) Ishitsuka, R., and Kobayashi, T. (2007) Cholesterol and lipid/protein ratio control the oligomerization of a sphingomyelin-specific toxin, lysenin. *Biochemistry* 46, 1495–1502.
- (37) Kiyokawa, E., Baba, T., Otsuka, N., Makino, A., Ohno, S., and Kobayashi, T. (2005) Spatial and functional heterogeneity of sphingolipid-rich membrane domains. *J. Biol. Chem.* 280, 24072–24084.
- (38) Baba, A., Akagi, K., Takayanagi, M., Flanagan, J. G., Kobayashi, T., and Hattori, M. (2009) Fyn tyrosine kinase regulates the surface

expression of glycosylphosphatidylinositol-linked ephrin via the modulation of sphingomyelin metabolism. *J. Biol. Chem.* 284, 9206–9214.

(39) Canals, D., Jenkins, R. W., Roddy, P., Hernandez-Corbacho, M. J., Obeid, L. M., and Hannun, Y. A. (2010) Differential effects of ceramide and sphingosine-1-phosphate on ERM phosphorylation: probing sphingolipid signaling at the outer plasma membrane. *J. Biol. Chem.* 285, 32476–32485.

(40) Hullin-Matsuda, F., Ishitsuka, R., Takahashi, M., and Kobayashi, T. (2009) Imaging lipid membrane domains with lipid-specific probes. *Methods Mol. Biol.* 580, 203–220.

(41) Brzoska, J. B., Shahidzadeh, N., and Rondelez, F. (1992) Evidence of a transition temperature for the optimum deposition of grafted monolayer coatings. *Nature* 360, 719.

(42) Wang, T., and Ikai, A. (1999) Protein Stretching III. Force-extension curves of tethered bovine carbonic anhydrase B to the silicon substrate under native intermediate and denaturing conditions. *Jpn. J. Appl. Phys.* 38, 3912–3917.

(43) Kiyokawa, E., Makino, A., Ishii, K., Otsuka, N., Yamaji-Hasegawa, A., and Kobayashi, T. (2004) Recognition of sphingomyelin by lysenin and lysenin-related proteins. *Biochemistry* 43, 9766–9773.

(44) Sekizawa, Y., Kubo, T., Kobayashi, H., Nakajima, T., and Natori, S. (1997) Molecular cloning of cDNA for lysenin, a novel protein in the earthworm Eisenia foetida that causes contraction of rat vascular smooth muscle. *Gene* 191, 97–102.

(45) Hutter, J. L., and Bechhoefer, J. (1993) Calibration of atomic force microscopy tips. *Rev. Sci. Instrum.* 64, 1868–1873.

(46) Kulma, M., Herec, M., Grudzinski, W., Anderluh, G., Gruszecki, W. I., Kwiatkowska, K., and Sobota, A. (2010) Sphingomyelin-rich domains are sites of lysenin oligomerization: implications for raft studies. *Biochim. Biophys. Acta* 1798, 471–481.

(47) Yuan, C., Furlong, J., Burgos, P., and Johnston, L. J. (2002) The size of lipid rafts: an atomic force microscopy study of ganglioside GM1 domains in sphingomyelin/DOPC/cholesterol membranes. *Biophys. J.* 82, 2526–2535.

(48) Maulik, P. R., and Shipley, G. G. (1996) N-palmitoyl sphingomyelin bilayers: structure and interactions with cholesterol and dipalmitoylphosphatidylcholine. *Biochemistry* 35, 8025–8034.

(49) Afrin, R., Alam, M. T., and Ikai, A. (2005) Pretransition and progressive softening of bovine carbonic anhydrase II as probed by single molecule atomic force microscopy. *Protein Sci.* 14, 1447–1457.

(50) Dufrene, Y. F., Barger, W. R., Green, J.-B. D., and Lee, G. U. (1997) Nanometer-scale surface properties of mixed phospholipid monolayers and bilayers. *Langmuir* 13, 4779–4784.

(51) Kunneke, S., Kruger, D., and Janshoff, A. (2004) Scrutiny of the failure of lipid membranes as a function of headgroups, chain length, and lamellarity measured by scanning force microscopy. *Biophys. J.* 86, 1545–1553.

(52) Barenholz, Y., Suurkuusk, J., Mountcastle, D., Thompson, T. E., and Biltonen, R. L. (1976) A calorimetric study of the thermotropic behavior of aqueous dispersions of natural and synthetic sphingomyelins. *Biochemistry* 15, 2441–2447.

(53) Needham, D., McIntosh, T. J., and Evans, E. (1988) Thermomechanical and transition properties of di-myristoylphosphatidylcholine/cholesterol bilayers. *Biochemistry* 27, 4668–4673.

(54) Demel, R. A., Jansen, J. W., van Dijck, P. W., and van Deenen, L. L. (1977) The preferential interaction of cholesterol with different classes of phospholipids. *Biochim. Biophys. Acta* 465, 1–10.